Available online at www.sciencedirect.com

SCIENCE DIRECT®

Thin Solid Films 468 (2004) 125–133

thin solid films

www.elsevier.com/locate/tsf

Room temperature pulsed laser deposited (Ti,Al)C_xN_{1-x} coatings—chemical, structural, mechanical and tribological properties

J.M. Lackner[a,b,c,*], W. Waldhauser[a], R. Ebner[a,b], R.J. Bakker[d], T. Schöberl[e], B. Major[f]

[a] *JOANNEUM RESEARCH Forschungsgesellschaft mbH, Laser Centre Leoben, Leobner-Strasse 94, A-8712 Niklasdorf, Austria*
[b] *Materials Center Leoben, Franz-Josef-Strasse 13, A-8700 Leoben, Austria*
[c] *Institute of Physical Metallurgy and Materials Testing, University of Leoben, Franz-Josef-Strasse 18, A-8700 Leoben, Austria*
[d] *Institute of Geological Sciences, University of Leoben, Peter-Tunner-Strasse 5, A-8700 Leoben, Austria*
[e] *Erich-Schmid-Institute, Austrian Academy of Sciences, Jahnstrasse 12, A-8700 Leoben, Austria*
[f] *Institute of Metallurgy and Materials Science, Polish Academy of Sciences, ul. Reymonta 25, 30-059 Cracow, Poland*

Received 23 October 2003; received in revised form 19 May 2004; accepted 19 May 2004
Available online 24 July 2004

Abstract

The aim of the present work was the improvement of titanium–aluminium nitride (TiAlN) coating by the solid-solution hardening with carbon atoms leading to titanium–aluminium carbonitride (Ti,Al)C_xN_{1-x} coatings with varying carbon (x) and nitrogen contents. The request of low deposition temperatures which are indispensable for the coating of heat-sensitive materials like tool steels of high hardness and polymers was reached by the application of the room temperature pulsed laser deposition (PLD) technique. A Nd:YAG laser of 1064 nm wavelength operated at two different laser pulse energies was used in the ablation experiments of pure TiAl targets (50 at.% Al) in various C_2H_2–N_2 gas mixtures. The results reveal a strong dependency of the gas mixture on the C and N content of the coatings. Furthermore, the different pulse energies change the ratio of Ti/Al atoms in the grown coatings. The crystallization was influenced too by the pulse energy and, thus, the energy and distribution of the atoms, ions and clusters. For the hardness and elastic moduli, two distinct stages in dependency on the crystallinity were found: High carbon contents lead due to the formation of pure carbon precipitations, found in the Raman investigations, to the destruction of the crystallin structure and, thus, to up to 60% lower hardnesses and elastic moduli. A low friction behaviour was found for coatings of the higher Al contents deposited at lower laser pulse energies due to the formation of carbon rich transfer layers on both the coatings and the Al_2O_3 counterparts.

PACS: 81.15 Fg; 46.55 +d
Keywords: Pulsed laser deposition; PLD; Laser ablation; Room temperature deposition; Titanium–aluminium carbonitride; TiAlCN; Hardness; Tribology; Structural Properties

1. Introduction

Over the past decade, the extension of service life of cutting and forming tools as well as of mechanical components has been successfully achieved by applying thin hard coatings onto their surfaces for reducing the wear and corrosion strains of the substrate materials. Titanium nitride (TiN) coatings deposited by different physical vapor deposition (PVD) and chemical vapor deposition (CVD) techniques are now widely accepted in a range of industrial applications with high demands in wear resistance and adhesion to the substrate [1,2]. However, there is mounting evidence that other transition metal nitrides and/or carbides may provide superior performance for some specific applications due to their higher hardness, higher high-temperature strength and higher corrosion resistance [3]. These materials have such properties due to their atomic bonding, which shows a mixed covalent, metallic and ionic character [4]. This bonding structure permits broad composition in binary and ternary solid solutions, achieved, e.g. in titanium carbide (TiC), titanium–aluminium nitride (TiAlN) or tita-

* Corresponding author. JOANNEUM RESEARCH Forschungsgesellschaft mbH, Laser Centre Leoben, Leobner-Strasse 94, A-8712 Niklasdorf, Austria. Tel.: +43-3842-81260-2305; fax: +43-3842-81260-2310.
E-mail address: juergen.lackner@joanneum.at (J.M. Lackner).

0040-6090/$ - see front matter © 2004 Elsevier B.V. All rights reserved.
doi:10.1016/j.tsf.2004.05.089

nium carbonitride (TiCN) coatings [5]. In addition, some authors showed further improvements of the mechanical and tribological performance by the addition of further elements like chromium, silicon, boron or carbon to these ternary coatings [5]. Exemplary, the solid solution hardening of TiAlN by the addition of carbon [6–8] seems to improve the mechanical and tribological behaviour of these ternary coatings. Some authors reported attractive properties of $(Ti,Al)C_xN_{1-x}$ coatings of varying contents of carbon (x) for milling operations at higher cutting speeds and dry working conditions [9,10] as well as for forging and aluminium diecasting [11]. Although the addition of carbon leads in cold-forming operations to a strong decrease in friction coefficients and an increase in hardness, the room temperature tribological behaviour of these coatings has not been investigated yet.

Furthermore, the present study combines the tribological characterization of $(Ti,Al)C_xN_{1-x}$ coatings with a low temperature deposition technique. This technique bypasses the two most important limitations of most of the PVD (e.g. magnetron sputtering, ion plating and arc discharge deposition) and (plasma-assisted) CVD processes used nowadays for the industrial manufactoring of hard coatings [12]: (1) For reaching sufficient adhesion to the substrate coating temperatures of at least 250 °C are required limiting the coating of thermal-sensitive substrates (e.g. distortion-sensitive parts) and substrate materials (e.g. polymers) [13]. (2) The application of bias voltage in DC configuration for increasing the adhesion even at temperatures lower than 250 °C is prevented by exactly these materials (polymers and other organic materials) due to their high electrical resistance leading to space-charge problems [14]. In contrast to most of the other PVD and CVD coating processes, the method applied in the present work—the pulsed laser deposition (PLD)—allows the coating of these materials in an industrial deposition process operating at room temperature [15–21]. In the PLD technique, a pulsed laser beam is focussed onto a target in order to evaporate its surface layers under vacuum or various process gas atmospheres [12]. The vaporized material consisting of atoms, ions and atomic clusters is subsequently deposited onto the substrate. The outstanding advantages of this technique are not only the possibilities to deposit thin films of very high chemical purity and excellent adhesion on various substrate materials even at room temperature but also high rate film growth on surface areas placed perpendicular to the irradiated target surface [16–18]. The application of reactive process like N_2 and C_2H_2 gases gives the opportunity of varying the chemical composition of the films in a wide range [12]. Thus, the (mechanical, tribological, electrical, optical, etc.) properties of the coatings can be tailored easily for their distinct application.

2. Experimental details

2.1. Film deposition

High purity Ti–Al targets (50 at.% Ti, 50 at.% Al, ratio of Ti/Al atoms (R) = 1) were taken for the ablation experiments using a pulsed Nd:YAG laser with 1064 nm wavelength and 10 ns pulse duration at a repetition rate of 10 Hz (Fig. 1) [22]. The pulse energy was set to 763 and 850 mJ pulse energy, respectively. The targets were rotated during the laser irradiation in order to avoid the formation of deep craters. The emitted species were deposited at room temperature in nitrogen containing C_2H_2 atmospheres onto quenched and tempered cold working steel substrates (AISI D2, hardness ~ 62 HRC) and molybdenum sheets, all with mirror-polished surfaces (roughness R_a ~ 3–4 nm). The different atmospheres (see Table 1) were chosen in order to produce $(Ti,Al)C_xN_{1-x}$ coatings with varying C and N contents. Prior to the film deposition, the substrates were cleaned ultrasonically in pure acetone and subsequently in ethanol. To increase the adhesion to the substrate, TiAl adhesive interface layers were deposited prior the growth of the hard coating materials as recommended by Lii et al. [23].

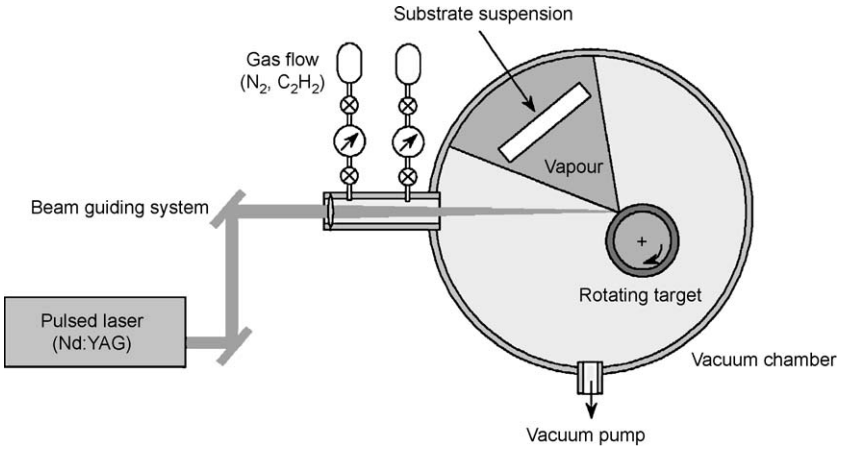

Fig. 1. Principle of the pulsed laser deposition (PLD) applied for tribological coating.

Table 1
Deposition parameters (laser pulse energy, C_2H_2 and N_2 gas flow) and properties (film thickness, adhesion, roughness) of the PLD (Ti,Al)C_xN_{1-x} coatings

Coating/ Sample	Laser pulse energy (m)	Gas flow (sccm)		Film thickness (μm)	Adhesion strength class [37]	Roughness, R_a (nm)
		C_2H_2	N_2			
C1	763	5	25	0.98	HF 1	7.86
C2	763	15	15	1.47	HF 2	5.57
C3	850	7.5	22.5	1.05	HF 2	8.57
C4	850	10	20	1.18	HF 1	7.02
C5	850	30	0	1.89	HF 1–2	5.37

2.2. Film characterization

Scanning electron microscopy (SEM, Cambridge Instruments Stereoscan 360) was applied for inspection of the surface quality, the growth structures at fracture sections and the wear scars of the coatings. This microscope is equipped with a wavelength dispersive spectroscopy analyser (WDS) for chemical analysis. The Raman spectra were obtained by means of a Dilor LABRAM confocal Raman spectrometer operated at a laser wavelength of 633 nm. The laser power of the He–Ne laser was 100 mW and the spot size was 5 μm. The spectra were taken between 160 and 1600 cm^{-1} with a resolution of 2 cm^{-1}. The phase composition of the (Ti,Al)C_xN_{1-x} coatings were analysed by an X-ray diffractometer (XRD, Bruker AXS D8 Discover) using grazing incidence (1.0°) of the primary beam (CuKα radiation). The texture analyses were performed using a Philips PW 1710 XRD X-ray diffractometer and CoKα radiation. Pole figure measurements were performed on a four-cycle goniometer equipment with a step size of 2.5° for the polar and azimuthal angle.

Atomic force microscopy (AFM) was applied for characterizing the surface structures on a nanometer scale using a Nanoscope III (Digital Instruments) facility in contact mode. The resolution of this equipment is about 1 nm in lateral and 0.2 nm in vertical direction. The hardness and elastic moduli of the coatings were determined by nanoindentation with a Vickers indenter using a Fischerscope H100. The applied maximum load was 10 mN, the loading rate was about 1 mN s^{-1} for all measurements. The indentation depth (~ 200 nm) was kept constant to prevent influences from the substrate and indentation size effects in testing the 0.98–1.89 μm thick coatings (Table 1).

The dry sliding friction behaviour of the coatings at room temperature (25 °C) and a relative humidity of about 60% was evaluated by a high-temperature ball-on-disc tribometer with 6 mm Al_2O_3 balls as counterparts. All experiments were carried out on the as-deposited, ultrasonically cleaned coating surfaces at a sliding speed of 0.1 m s^{-1} and an applied load of 2 N on a circle of 12 mm diameter. Optical profilometry (Veeco NT-1000) was used to inspect the wear tracks for analysing the wear mechanisms and the wear coefficients as well as for the roughness measurements.

3. Results and discussion

3.1. Chemical composition of the coatings

In the quantitative chemical analyses of the coatings by means of WDS two influences of the deposition parameters on the chemical composition were obtained (Fig. 2):

(1) The ratio of Ti/Al atoms (R) is in all coatings higher than in the target ($R=1$) (Fig. 2a). This may be a result of different degrees of interactions between the ablated species and the gas molecules in the vacuum chamber during the flight phase between the target after ablation and the substrate surfaces [12]. Due to the lower atomic mass of Al ($m_{Al}=26.98$ g mol^{-1}) compared to Ti atoms ($m_{Ti}=47.88$ g mol^{-1}), the Al species suffers higher scattering in the collisions with these gas molecules (N_2, C_2H_2) during the flight phase leading to a lower volume density of Al in the vapour [24]. Thus, the deposition rate of Ti atoms on the substrate surface is higher than for Al resulting in $R>1$. In contrast, the different contents of C_2H_2 and N_2 in the gas atmosphere during deposition scarcely influence this phenomenon due to the nearly equal molecular weights of C_2H_2 and N_2 molecules.
The application of higher laser pulse energies (laser fluences) increases the Ti contents in the coatings too (Fig. 2a). A possible explanation for this behaviour could be higher resputtering rates of Al atoms at the substrate surface at higher ion energies [25]. A similar behaviour was reported for Al atoms in TiAlN film

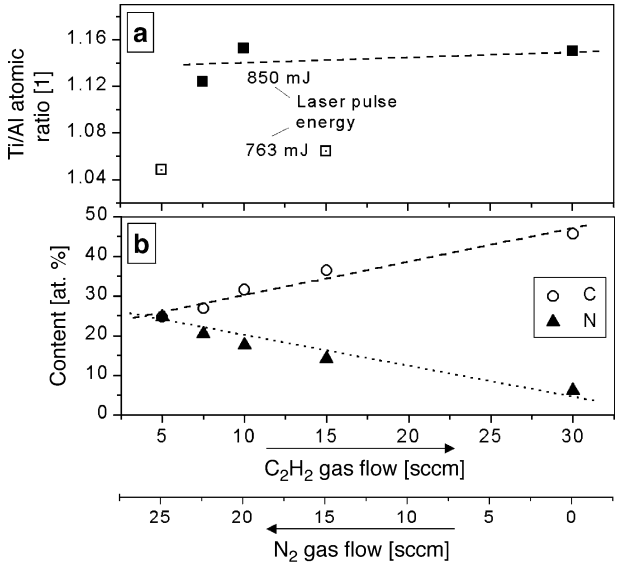

Fig. 2. Chemical composition of the (Ti,Al)C_xN_{1-x} coatings in dependency on the C_2H_2 and N_2 gas flows applied for deposition: (a) atomic ratio of Ti/Al (pulse energy: □ 763 mJ, ■ 850 mJ); (b) atomic content of carbon and nitrogen.

deposition [26,27] decreasing the Al deposition rate and increasing R.

(2) The composition of the gas atmosphere depending on the C_2H_2 and N_2 gas flows during deposition leads to strong influences on the content of carbon and nitrogen atoms in the coatings (Fig. 2b). Thus, it seems to be clear that the collisions of the Ti and Al species (atoms, ions and clusters) with the reactive gas molecules (N_2, C_2H_2) in the vacuum chamber during the flight phase result not only in the scattering of these ablated species but also in a significant ionization of the process gas necessary for chemical reactions with the ablated species both in the flight phase and on the substrate surface [12]. An increase of the C_2H_2 or N_2 gas flow results in a nearly linear increase of the C and N content of the coating, respectively (Fig. 2b). The higher reactivity of C_2H_2 molecules in comparison to N_2 molecules can be found in the higher carbon content in the coatings even at lower C_2H_2 gas flows. The remaining N_2 content after evacuation of the vacuum chamber is responsible for the low nitrogen content in the coating C5 deposited in the nearly pure C_2H_2 atmosphere.

The application of Raman spectroscopy enables the interpretation of the bonding in the (Ti,Al)C_xN_{1-x} coatings. Fig. 3 shows the Raman spectra of all coatings deposited and the substrate material. First of all, influences of the substrate on the Raman spectra of the coatings seem to be neglected due to high absorption of the coatings in the spectral range (633 nm) of the He–Ne laser and high coating thickness (Table 1). The comparison of the spectra of the (Ti,Al)C_xN_{1-x} coatings with Raman shifts of peak maxima obtained in investigations of TiAlN and TiCN coatings [28,29] reveals the structural change from the TiAlN to the TiCN type at higher C_2H_2 flows during deposition (higher C contents of the films). In the coatings C1 and C3 with the lowest carbon contents, a broad peak between Raman shifts of 500 and 800 cm^{-1} can be obtained, which is diminished at higher carbon contents

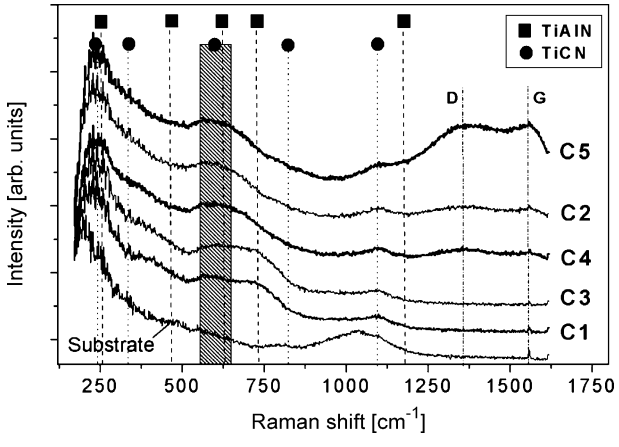

Fig. 3. Raman spectra of the (Ti,Al)C_xN_{1-x} coatings and the AISI D2 substrate material containing the standard values for TiAlN [28,29] and TiCN [28] as well as for sp^3 bonded (D) and sp^2 bonded (G) carbon [30].

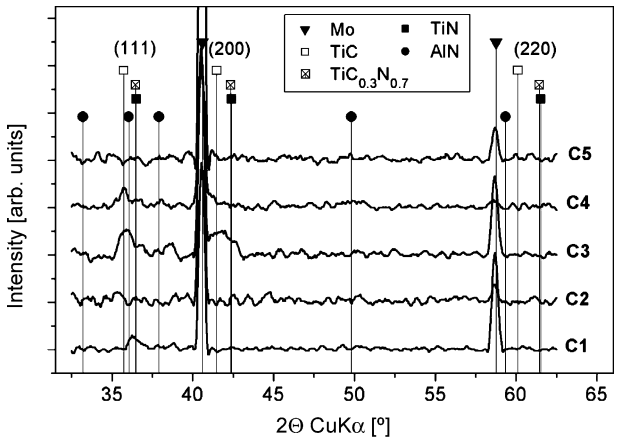

Fig. 4. Glancing angle (1.0° incidence of the primary beam) XRD spectra of the (Ti,Al)C_xN_{1-x} coatings. For comparison, the diffraction patterns [33] of TiC, $TiC_{0.7}N_{0.3}$, $TiC_{0.3}N_{0.7}$, TiN, AlN for the coatings and Mo for the substrate material applied are marked.

(coating C4, C2, C5). Instead of this peak, a broad peak occurs between 550 and 650 cm^{-1} in the Raman investigations of the latter coatings. The peak at about 1100 cm^{-1} relatable to TiCN [28] can be observed in all coatings. Furthermore, high carbon contents in the coatings result in the formation of sp^2 (graphite-like, G) and sp^3 (diamond-like, D) bonded carbon atoms [30] which are found in the coatings C4, C2 and predominating in coating C5. The D and G peaks found for these coatings reveal pure carbon precipitations or cluster boundaries in this coating [31,32].

3.2. Microstructure of the coatings

Grazing incidence XRD analysis of the (Ti,Al)C_xN_{1-x} coatings show for coatings with lower carbon contents (coating C1, C3, C4) crystalline structures, whereas the other coatings (C2, C5) seem to be amorphous (Fig. 4). The identification of the peaks leads to phases with fcc structures similar to TiN or TiC [33]. This structures were expected due to the well known high solubility of Al and C in the fcc NaCl-like TiN lattice [27], which can be attributed to the very similar atomic radii of Ti and Al as well as of C and N [34]. The higher the content of the smaller Al and C atoms (compared to Ti and N, respectively), the higher the shift to lower diffraction angles is. A further influence on the position of the peak maxima of the diffraction pattern is evident due to stresses in the coatings. Compressive stresses result in a shift to lower diffraction angles and interfere the shift caused by the chemical composition. Such stresses are very characteristic for PVD coatings and are caused by differences in the thermal expansion of the substrate and the coatings (if deposited at elevated temperatures) and by the growth of the coatings [35], which are also present in room temperature deposited coatings. Due to these two phenomena, a calculation of the lattice stresses in the films is not possible from XRD analyses. Nevertheless, a qualitative comparison of the crystalline coatings C1, C3 and C4 showed a much higher

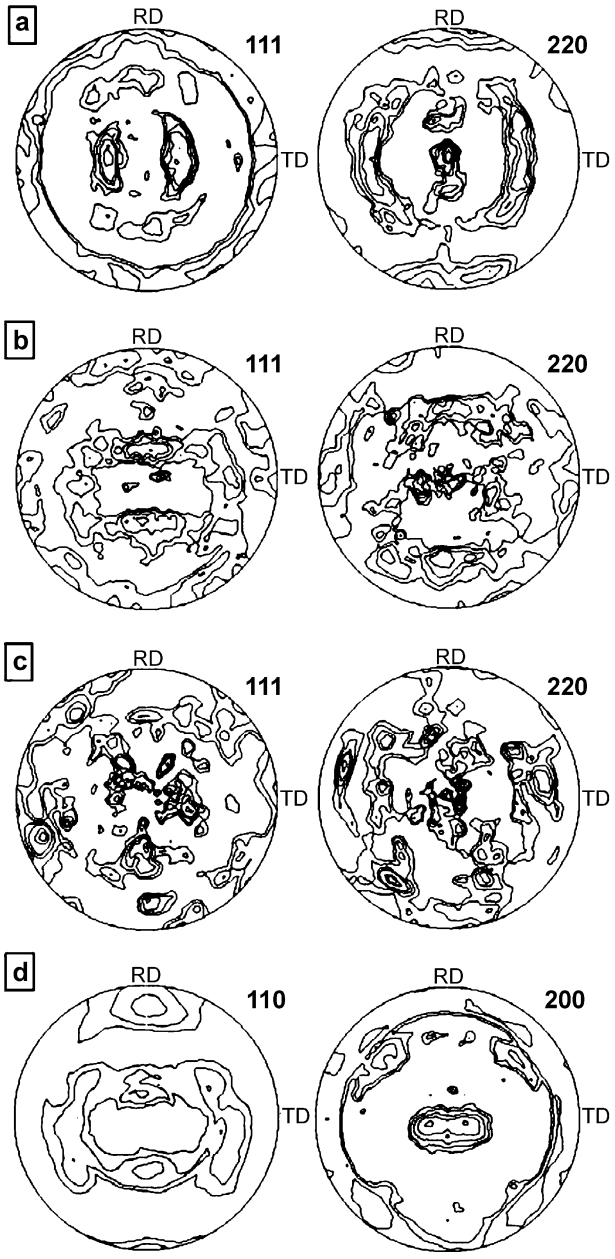

Fig. 5. Pole figures of the (Ti,Al)C_xN_{1-x} coatings: (a) C1, (b) C3, (c) C4 and (d) the Mo substrate.

shift to lower diffraction angles of the (111) peak of the two latter coatings deposited at the higher laser pulse energy of 850 mJ. It is obvious that higher pulse energies result in a higher degree of ionization of the vapour [25] and, thus, in higher average energies of the species at the substrate surface [36]. These higher energetic species can penetrate much deeper in the growing film, ending up in higher lattice mismatch and higher compressive stresses. A similar behaviour was found for TiN coatings [17]. Besides the higher compressive stresses in the coatings deposited at higher laser pulse energy the (200) peak of TiN and TiC, respectively, can be obtained in coating C3. The arise of this peak in the fcc lattice is always connected with very high energetic particles. According to Lüth et al. [37], the (200) lattice planes are able to incorporate high energetic ions without large mismatches of the lattice by the "channelling" mechanism. This mechanism allows the slowing of ions in small portions by scattering with several atomic layers along distinct channels in (200) directions. Thus, resputtering is scarcely found in the case of (200) crystallites, whereby the growth of this grains is not hindered. If the ion bombardment is weaker, the growth of {111} or {220} lattice planes (with lower surface energies than {200} planes) parallel to the substrate surfaces is favoured which was found for all other crystalline coatings.

Pole figures measurements (Fig. 5) reveal the different preferred orientations of the lattice planes parallel to the surface. According to the XRD investigations, the coating C3 (Fig. 5b) possesses a distinct (111) structure of the fcc lattice slightly moved out of the centre of the pole figure. The other crystalline coatings possess the distinct fiber textured structures too, which are characteristically for Ti-based PLD coatings [17,19], but due to the lower energetic film growth the main lattice orientation is (220) (Fig. 5a,c). The missing of this lattice component in the XRD spectra is a result of the strong texture. Influences of the texture of the molybdenum substrate on the coatings texture can be excluded due to the application of TiAl adhesive interfaces and very different rolling texture of the substrate ({101}⟨011⟩) (Fig. 5d). Compared to earlier investigations on TiAlN coatings [19], similar (111) textures were found in the present study, except for the coating C3.

The decrease in the intensity of the XRD patterns of the coatings C4 and the lost of XRD patterns of the coatings C2 and C5 with the highest carbon content and, thus, the appearance of amorphous structures can be attributed to the growth of highly carbon containing precipitations or cluster boundaries [32] and the increase of the hydrogen content of the deposition atmosphere which probably increases the hydrogen content in the coatings. SEM investigations of fracture sections of these coatings reveal the amorphous microstructure, whereas all crystalline coatings (C1, C3, C4) present a very fine grained structure (Fig. 6a) similar to the zone-T structure of Thornton's structure zone model [38].

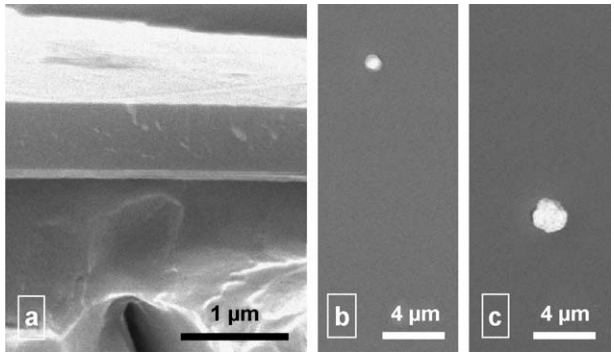

Fig. 6. SEM images of (a) the fracture section of coating C1, (b) the surface of coating C3 and (c) the surface of coating C5 showing different shapes of particulates.

3.3. Topography of the coatings

Light microscopic investigations of the coating surfaces showed low densities of defects between 9×10^3 and 11×10^3 cm^{-2}, which are independent on the coating composition. These defects originate in the ablation of the target by the pulsed laser irradiation, in which apart from vapourized atoms, ions and clusters also molten droplets and solid particles are ejected [12]. Both types of surface defects were found in the SEM investigations of the different coating surfaces: On the surfaces of $(Ti,Al)C_xN_{1-x}$ coatings deposited at the lower C_2H_2 contents in the vacuum chamber (C1, C3) mainly round-shaped droplets were found (Fig. 6b). In contrast, the surfaces of the coatings C2 and C5 deposited at the higher C_2H_2 gas flows present spattered particulates (Fig. 6c) which are caused by redeposited layers around the ablation spot on the target surface [22]. Due to the rotation of the target, these brittle layers split off by subsequent laser pulses because of their different thermomechanical and optical behaviour compared to the metallic target material below them [22]. On the surface of the coating C4 about the same amount of both shapes of droplets was found. Thus, this coating seems to represent a transition stage between the two ablation and deposition characteristics. The size of all these defects is ranging between 0.5 and 2.5 μm. Thus, about 99% of the substrate surfaces are free of droplets and particulates.

Detailed investigations of the surfaces on a nanometer scale were performed by means of AFM. Representing the two $(Ti,Al)C_xN_{1-x}$ coatings of the lower carbon contents (C1, C3), the surface image of coating C1 (Fig. 7a) shows some small clusters (density ~ 7 μm^{-2}) of about 10–15 nm height and 100–200 nm diameter. The density of these clusters is decreased (~ 2–3 μm^{-2}) on the surfaces of the coatings of high carbon content (e.g. C2, Fig. 7b). Thus, relations between the crystallinity and the cluster density seem to be possible. In this case, the clusters are the tops of crystalline micro-columns in the coating, which are embedded in an amorphous matrix [32]. Considering the low peak intensity of the XRD patterns of the crystalline coatings (C1, C3, C4) in the glancing angle diffraction arrangement, the high volume of amorphous phases between the crystalline clusters seems to be predictable. The different densities of the surface clusters influence the surface roughness R_a

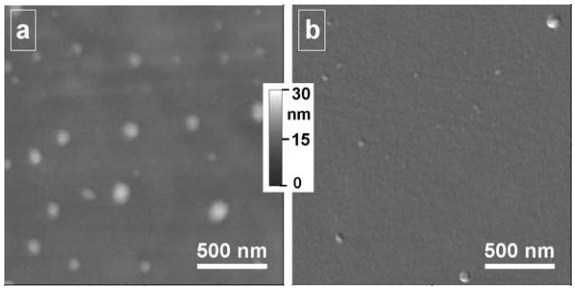

Fig. 7. AFM micrographs of (a) coating C1 and (b) C2.

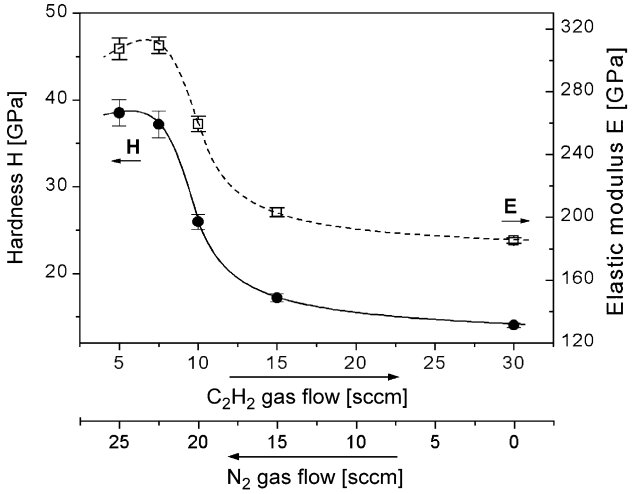

Fig. 8. Dependency of the hardness and the reduced elastic modulus on the C_2H_2 and N_2 gas flows applied in the ablation experiments.

(Table 1), found in optical profilometry imaging of 5350 μm^2 large areas. The higher roughnesses ($R_a \sim 7$–8.6 nm) were found for the coatings of crystalline structure (C1, C3, C4), the highest value occurs for the coating C3 with the highest diffraction patterns and, thus, highest degree of crystallinity. The low roughnesses ($R_a \sim 5.5$ nm) of the coatings with the highest carbon content (C2, C5) correspond to the very low density of clusters on the coating surfaces.

3.4. Mechanical properties and adhesion

The mechanical behaviour of the $(Ti,Al)C_xN_{1-x}$ points out the influence of crystallinity and chemical composition, too. For both properties, hardness and reduced elastic modulus, a similar decrease was found for increasing C_2H_2 gas flows during deposition, which are directly related to the carbon and nitrogen contents in the coatings (Fig. 2b). At low carbon contents, high hardness as well as high elastic moduli were found which can be related to a solid solution hardening of the (Ti,Al)N lattice with carbon atoms (Fig. 8). Earlier investigations of carbon-free PLD (Ti,Al)N coatings [19] showed a hardness of about 32.2 GPa and a reduced elastic modulus of about 313 GPa for similar deposition conditions (pulse energy: 763 mJ, N_2 gas flow: 30 sccm, N content of the coating: ~ 42.5 at.%). Thus, it can be obtained that the incorporation of low concentrations of carbon atoms scarcely influences the elastic moduli, but significantly increases the hardness. Obviously, after the exceeding of a maximum concentration of solutable carbon (~ 25 at.%) at C_2H_2 flows of about 6–7 sccm, a reduction of both the hardness and the elastic moduli to less than the halve and to about 2/3, respectively, can be obtained. The low level of both mechanical properties corresponds to the amorphous structure of these coatings (C2, C5). Furthermore, the decrease in crystallinity of coating C4 (10 sccm C_2H_2) compared to C1 and C3, respectively, fits well with

the transition stage of the mechanical behaviour. Besides the lost of crystallinity of the coatings C2 and C5, the appearance of a high amount of C–C bonds (sp^2 bonding in graphite, sp^3 bonding in diamond) is evident at the high C_2H_2 gas flows, as mentioned above in the Raman investigations (Fig. 3). Observing the low hardness level, a high amount of sp^2 bonded carbon and relatively high hydrogen contents can be expected for these coatings [30].

The adhesion of the (Ti,Al)C_xN_{1-x} coatings on the AISI D2 tool steel substrates (hardness ~ 62 HRC) was tested by means of the Rockwell indentation test [39]. This test is based on the indentation of a Rockwell-C diamond in the coated substrate material with a base hardness between 54 and 65 HRC and a coating thickness between 1 and 4 μm. The adhesion strength is classified afterwards qualitatively in the plastically deformed surroundings of the indentation by light microscopy. Six classes of adhesion (HF1–HF6) are defined the DIN standard [39] according to the damage, of which the first four classes (HF1–HF4) allow the application of the coating on industrially used tools. All coatings deposited in the current work possess very high adhesion strength (HF1 and HF2) due to the use of adhesive TiAl interfaces [23]. These two classes correspond to only very few cracking and the missing of coating delaminations in the plastically deformed surroundings of the Rockwell indents.

3.5. Tribological behaviour of the coatings

Due to the high adhesion of the (Ti,Al)C_xN_{1-x} coatings to the substrate surfaces, an excellent tribological behaviour of the coatings was found in the ball-on-disc test against Al_2O_3 counterparts. No coating failure was found after a sliding distance of 200 m of the alumina balls on the as-deposited coating surfaces. Thus, the evaluation of the dependency of the friction coefficients on the sliding distance showed only two distinct stages, e.g. shown for coating C5 in Fig. 9: (1) The first, very short stage I can be attributed to the run-in period, in which the cracking of roughness tips on both counterparts and a breakout of coating defects occur leading to the formation of wear debris. The friction coefficients were found in all cases

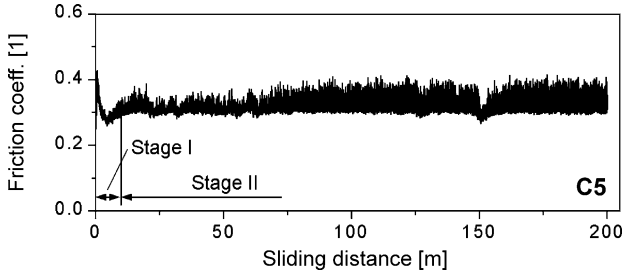

Fig. 9. Dependency of the friction coefficient on the sliding distance in the ball-on-disc test of coating C5 (tribological test parameters: temperature: 25 °C, humidity: 60%, counterpart: Al_2O_3, friction load: 2 N, sliding diameter: 12 mm).

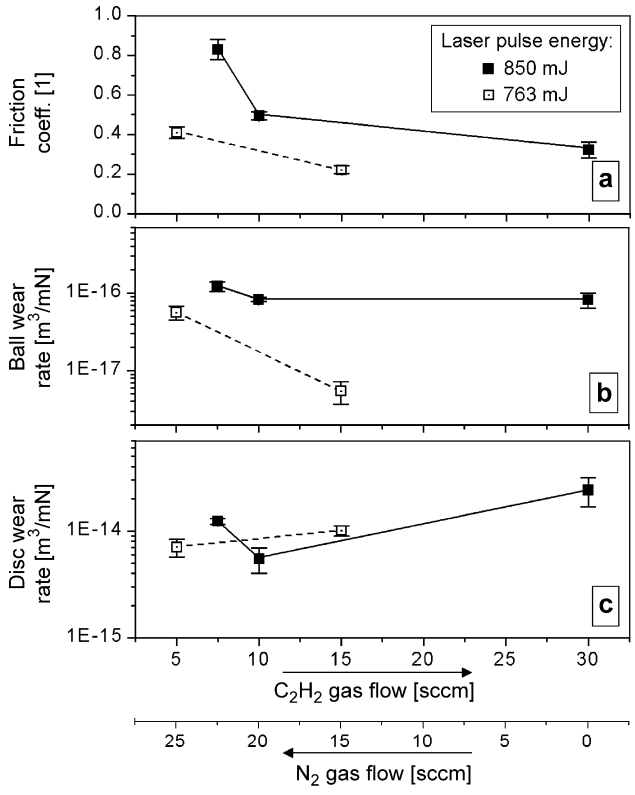

Fig. 10. (a) Friction coefficient, (b) ball wear rate and (c) disc wear rate in dependency on the C_2H_2 and N_2 gas flow applied for deposition (pulse energy: □ 763 mJ, ■ 850 mJ) (tribological test parameters: temperature: 25 °C, humidity: 60%, counterpart: Al_2O_3, friction load: 2 N, sliding diameter: 12 mm, sliding distance: 200 m).

starting from a very low level (0.15–0.30) in the first contact, but rapidly increasing to values up to 0.4–1.0 followed by the decrease down to the friction coefficient of stage II. (2) Stage II can be defined as the steady-state friction period and starts after the drop of the friction coefficients from the maximum values in stage I after about 10–25 m of sliding. The friction coefficients in this stage are very dependent on the coating type, as shown in Fig. 10a: For the coatings deposited at the lower laser pulse energy (763 mJ) (C1, C2), a low friction behaviour was found in contrast to the other coatings. An increase of the carbon content resulted in a decrease of the friction coefficient for both laser pulse energies applied in the ablation experiments. Compared to TiAlN coatings deposited earlier by means of PLD [19], the addition of even low carbon contents results in the reduction of friction coefficients from 1.0 to about 0.4–0.86.

Due to the lower friction coefficients, the ball wear rates of the coatings deposited at 763 mJ are lower than for the other coatings (Fig. 10b). In contrast, no significant influences of the laser pulse energy during deposition on the disc wear rate were found (Fig. 10c). Only the chemical composition and hardness, respectively, seem to influence the wear of the (Ti,Al)C_xN_{1-x} coatings: Higher carbon contents and, thus, lower hardness lead to higher disc wear.

Comparing the wear behaviour of the PLD (Ti,Al)C_xN_{1-x} coatings with other PLD coatings deposited earlier (e.g. TiN, TiAlN, TiO_2 [16–19]), the wear rates found are on the same level or higher.

To find the reasons for the different tribological behaviour of the coatings deposited at different laser pulse energies, detailed studies of the worn surfaces were performed by means of optical profilometry and Raman spectroscopy. In agreement with the results of the ball-on-disc tests, two different phenomena were found (Fig. 11):

(1) The wear tracks of the low-friction coatings C1 and C2 grown at the lower pulse energy of 763 mJ (e.g. C2 in Fig. 11a) are covered with a thick transfer layer. This transfer layer contains a high contents of carbon atoms (graph A in the Raman spectra in Fig. 11c) with a higher degree of sp^3 hybridization than found for the unworn coating near the wear track (Fig. 3). It is apparent in the optical profilometry image as well as in the SEM image of the wear track in Fig. 11a that the transfer layer covers only the centre part of the wear track (area A), whereas the smooth rims (area B) possess the same chemical composition than the coatings itself (graph B in Fig. 11c).

(2) For the coatings deposited at the higher pulse energy of 850 mJ (C3, C4, C5), the formation of a transfer layer cannot be observed, as shown for coating C3 in Fig. 11b. In the case of these coatings, only wear debris of low adhesion, leading to the peaks in the optical profilometry image, were found in the wear scars. The Raman studies of these wear tracks confirm the absence of carbon containing transfer layers and a chemical composition of the wear tracks (graph C in Fig. 11c) equal to the unworn coating surfaces (see Fig. 3).

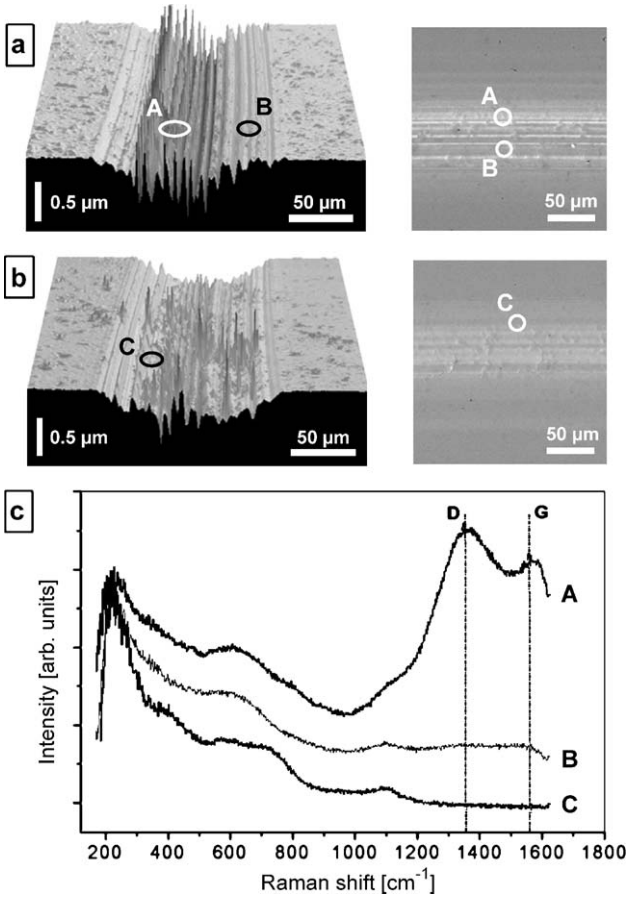

Fig. 11. Topographical optical profilometry and SEM images of (a) the disc wear track of coating C2 and (b) coating C3. The points marked with A, B and C, respectively, are related to surface areas on which the Raman spectra, shown in (c), were measured.

Discussing the influences on the tribological behaviour, only significant differences in the ratio of Ti/Al atoms in the coatings were found for the two different laser pulse energies used in the ablation experiments. Influences of the laser pulse energy on the hardness, the elastic modulus and the microstructure are not as high as the influences on the chemical composition. Due to the high temperatures during the tribological contact to the alumina counterpart and the ambient air atmosphere used, the bonding structure in the wear track of the (Ti,Al)C_xN_{1-x} coatings can change. Evidences for such reactions can only be found for the coatings of low Ti/Al atomic ratios by comparison of the Raman spectra in Fig. 11. Thus, it seems to be possible that the formation of carbon-rich Al compounds (e.g. Al_4C_3) occurs at higher Al contents in the coatings (coatings C1 and C2). Such Al–C compounds are unstable in humid atmospheres [28] and decompose to carbon (or C-rich compounds), forming the transfer layer, and Al (or Al-rich compounds), reacting in subsequent tribological contacts with N atoms, e.g. The low-friction range is reached, if the transfer of carbon from the soft surface of the coatings wear track to the counterpart starts. Thus, sliding occurs only on these carbon layers. These transfer layers on the counterparts were found only in the light microscope investigations of the alumina balls sliding on the coatings C1 and C2 after reaching the low-friction range.

4. Conclusions

(Ti,Al)C_xN_{1-x} coatings were deposited by means of the pulsed laser deposition (PLD) technique from a TiAl target with a Nd:YAG laser (wavelength: 1064 nm) in atmospheres of different C_2H_2 and N_2 reactive gas mixtures at room temperature. The variation of the gas mixture strongly influences the carbon and nitrogen content of the coatings. The atomic ratio of Ti/Al was found dependent on the laser pulse energy used in the ablation experiments. At the higher pulse energies used, higher Ti contents in the coatings were found. Furthermore, the higher pulse energy leads to higher energies of the ablated and subsequently deposited species resulting in higher crystallinity of the coatings. High carbon contents in

the coatings result in X-ray amorphous microstructures. The lost of crystallinity influences the mechanical behaviour, too. A decrease to less than 50% of the hardness of low carbon containing, crystalline and, thus, solid-solution hardened $(Ti,Al)C_xN_{1-x}$ coatings ($\sim$ 40 GPa) can be obtained for the amorphous coatings. The decrease of the elastic modulus of these coatings was found to be about 30% compared to crystalline types. AFM investigations of the very smooth ($R_a \sim 5-8.6$ nm) and nearly particulate-free coating surfaces revealed effects of the crystallinity on the number and size of nano-clusters, which seem to be the tops of crystalline microcolumns. Due to the low diffraction patterns found in the glancing angle XRD investigations, these crystalline microcolumns seem to be embedded in an amorphous matrix. Higher carbon contents in the coatings lead to the formation of carbon precipitations or cluster boundaries found in the appearance of peaks of sp^2 and sp^3 bonded C atoms in the Raman spectra which prevent in combination with the hydrogen the crystallization of the coatings at the low temperatures (25 °C) applied for deposition. Due to the use of metallic TiAl interlayers as well as the highly ionized vapour which is characteristic for the PLD process, excellent adhesion of the coatings was found. The tribological performance is mainly influenced by the differences in the ratio of Ti/Al atoms. A low friction behaviour (friction coefficient $\sim$ 0.2) is found only for coatings deposited at the lower pulse energy due to the formation of graphite transfer layers on the wear tracks of both the coating and the alumina counterpart. Possibly, the formation of Al–C compounds, which are unstable in humid atmospheres (relative humidity during ball-on-disc test $\sim$ 60%), influences the growth of the transfer layer growth, which is not present on the coatings deposited at the higher laser pulse energy. The low-friction behaviour decreases the wear rates of the Al_2O_3 counterpart, whereas no significant influences on the coatings wear rates were found.

Acknowledgement

Financial support of this work by the "Theodor-Körner-Fonds zur Förderung von Wissenschaft und Kunst" of the "Kammer für Arbeiter und Angestellte Wien" is highly acknowledged. Further financial support was provided by the Austrian Federal Ministry of Traffic, Innovation and Technology, the Austrian Industrial Research Promotion Fund (FFF), the Government of Styria, the Technologie Impulse Gesellschaft mbH in the frame of the Kplus Programme and the European Union.

References

[1] M.Y. Al-Jaroudi, H.T.G. Hentzell, S. Gong, A. Bergton, Thin Solid Films 195 (1991) 63.
[2] H.Z. Wu, T.C. Chou, A. Mishra, D.R. Anderson, J.K. Lampert, C. Gujrathi, Thin Solid Films 191 (1991) 55.
[3] L.E. Toth, Refractory Materials, vol. 7, Academic Press, New York, 1971.
[4] J.-E. Sundgren, H.T.G. Hentzell, J. Vac. Sci. Technol., A, Vac. Surf. Films 4 (1986) 2259.
[5] K. Holmberg, A. Matthews, Coatings Tribology, Elsevier, Amsterdam, 1994.
[6] O. Knotek, F. Löffler, L. Wolkers, Surf. Coat. Technol. 68/69 (1994) 176.
[7] D. Heim, R. Hochreiter, Surf. Coat. Technol. 98 (1998) 1553.
[8] K. Kawata, H. Sugimura, O. Takai, Thin Solid Films 390 (2001) 64.
[9] O. Knotek, M. Böhmer, T. Leyendecker, J. Vac. Sci. Technol., A, Vac. Surf. Films 4 (1986) 2695.
[10] W.-D. Münz, J. Vac. Sci. Technol., A, Vac. Surf. Films 4 (1986) 2717.
[11] E. Bernacchi, A. Ferrero, E. Gariboldi, A. Korovkin, G. Pontini, Metall. Sci. Technol. 14 (1996) 3.
[12] D.B. Chrisey, G.K. Hubler, Pulsed Laser Deposition of Thin Films, John Wiley & Sons, New York, 1994.
[13] V. Sedlacek, Metallic Surfaces, Films and Coatings, Elsevier, Amsterdam, 1992.
[14] B. Rother, J. Vetter, Plasmabeschichtungsverfahren und Hartstoffschichten, Deutscher Verlag für Grundstoffindustrie, Leipzig, 1992.
[15] R. Ebner, W. Waldhauser, W. Lenz, Proc. Materials Week 2001, München, Germany, DGM, Frankfurt, Germany, 2001.
[16] J.M. Lackner, W. Waldhauser, R. Ebner, W. Lenz, B. Major, T. Schöberl, Sonderbd. Prakt. Metallogr. 34 (2003) 291.
[17] J.M. Lackner, W. Waldhauser, R. Ebner, B. Major, T. Schöberl, Thin Solid Films 181–181C (2003) 585.
[18] J.M. Lackner, W. Waldhauser, R. Ebner, B. Major, T. Schöberl, Surf. Coat. Technol. 180–181 (2004) 585.
[19] J.M. Lackner, W. Waldhauser, R. Ebner, J. Keckés, T. Schöberl, Surf. Coat. Technol. 177–178 (2004) 447.
[20] J.M. Lackner, C. Stotter, W. Waldhauser, R. Ebner, W. Lenz, M. Beutl, Surf. Coat. Technol. 174–175 (2003) 402.
[21] J.M. Lackner, W. Waldhauser, R. Ebner, W. Lenz, W. Mroz, Galvanotechnik 5 (2003) 1226.
[22] J.M. Lackner, Innovative Coating by Pulsed Laser Deposition, PhD thesis, University of Leoben, Austria, 2003.
[23] D.-F. Lii, J.-L. Huang, M.-H. Lin, Surf. Coat. Technol. 99 (1998) 197.
[24] R. Wuhrer, W.Y. Yeung, Scr. Mater. 49 (2003) 199.
[25] T. Witke, T. Schuelke, J. Berthold, C.F. Meyer, B. Schultrich, Surf. Coat. Technol. 116–119 (1999) 609.
[26] D.-Y. Wang, Y.-W. Li, C.-L. Chang, Surf. Coat. Technol. 114 (1999) 109.
[27] S. PalDey, S.C. Deevi, Mater. Sci. Eng., A Struct. Mater.: Prop. Microstruct. Process. 342 (2003) 58.
[28] C.P. Constable, J. Yarwood, W.-D. Münz, Surf. Coat. Technol. 116–119 (1999) 155.
[29] K.N. Jallad, D. Ben-Amotz, Wear 252 (2002) 956.
[30] J. Robertson, Mater. Sci. Eng., R Rep. 37 (2002) 129.
[31] Y.L. Su, W.H. Kao, Wear 236 (1999) 221.
[32] P. Panjan, M. Cekada, D. Kek Merl, M. Macek, Vacuum 71 (2003) 261.
[33] Powder Diffraction File, Joint Committee on Powder Diffraction Standards, International Centre for Diffraction, Philadelphia, PA, 2002.
[34] F.A. Cotton, G. Wilkinson, P.L. Gaus, Basic Inorganic Chemistry, John Wiley & Sons, New York, 1987.
[35] C. Hudson, R.E. Somekh, J. Vac. Sci. Technol., A, Vac. Surf. Films 14 (1996) 2169.
[36] S. Amoruso, Appl. Surf. Sci. 138–139 (1999) 292.
[37] H. Lüth, Surfaces and Interfaces of Solid Materials, Springer, Berlin, 1995.
[38] J.A. Thornton, J. Vac. Sci. Technol. 11 (1974) 666.
[39] H. Jehn, G. Reiners, N. Siegel, DIN-Fachbericht, vol. 39, Beuth-Verlag, Berlin, Germany, 1993.